Changes in Local Structure during Electrochemical Li Insertion into A-Site Deficient Perovskite Oxides, La$_{1/3}$NbO$_3$

Masanobu Nakayama, Hiromasa Ikuta, Yoshiharu Uchimoto, and Masataka Wakihara*

Department of Applied Chemistry, Tokyo Institute of Technology, Ookayama,
Meguro-ku, Tokyo 152-8552, Japan

Yasuko Terada

Japan Synchrotron Radiation Research Institute, Spring-8, 1-1-1 Kouto Mikazuki-cho,
Sayo-gun, Hyogo, 679-5198, Japan

Takafumi Miyanaga

Department of Materials Science and Technology, Faculty of Science and Technology, Hirosaki University,
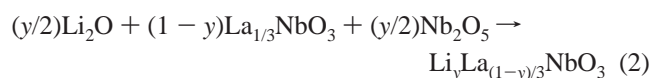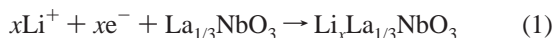*Hirosaki, Aomori, 036-8561, Japan*

Iwao Watanabe

Faculty of Science, Osaka Women's University, 2-1 Daisan-cho, Sakai, Osaka 590-0035, Japan

A detailed investigation of the local structural changes with lithiated perovskite oxides, Li$_x$La$_{1/3}$NbO$_3$, has been carried out using extended X-ray absorption fine structure (EXAFS) measurements. From Nb K-edge EXAFS measurement, the interatomic distance of first shell Nb−O interaction increased with the composition *x* by electrochemical Li$^+$ insertion. This behavior ascribed to the expansion of Nb ion due to the reduction of Nb^{5+} to Nb^{4+}. On the other hand, La K-edge EXAFS measurement showed that the interatomic distance of the first shell La−O interaction decreased with the lithiation reaction. Furthermore, those of second shell Nb−La and third shell Nb−Nb and La−La bonds tended to be unchanged with reaction. Such a complicated behavior in the change of each interatomic distance with lithium insertion can be understood by the model of tilting of NbO$_6$ octahedra in the perovskite structure.

Introduction

Transition-metal oxides having lithium insertion sites are particularly interesting as cathode and anode materials for lithium ion batteries with high-energy density.[1,2] These materials are attractive not only for practical use but also for model materials in basic study of solid-state electrochemical reactions. Since the host crystal structure is almost the same before and after electrochemical insertion reaction, these model materials are suitable for theoretical treatment, such as first principles molecular orbital calculation,[3−7] lattice gas model simulation,[8] and so on.[9,10] A-site deficient perovskite oxide, La$_{1/3}$NbO$_3$, is considered to be one of the candidates as a model compound, because there are a large number of vacancies to insert Li ions. In addition, it is known that there are two types of lithium insertion reaction into La$_{1/3}$NbO$_3$: one is the electrochemical Li$^+$ insertion reaction (eq 1)[11,12] and the other is the thermal Li$^+$ insertion reaction (eq 2).[13,14] (The latter one is considered more accurately as the substitution of Li$^+$ for La^{3+} in perovskite A-site.)

$$x\text{Li}^+ + xe^- + \text{La}_{1/3}\text{NbO}_3 \rightarrow \text{Li}_x\text{La}_{1/3}\text{NbO}_3 \qquad (1)$$

$$(y/2)\text{Li}_2\text{O} + (1-y)\text{La}_{1/3}\text{NbO}_3 + (y/2)\text{Nb}_2\text{O}_5 \rightarrow$$
$$\text{Li}_y\text{La}_{(1-y)/3}\text{NbO}_3 \quad (2)$$

Therefore, by comparing these two reactions, the relevant knowledge for the Li insertion reaction was expected to be

available, and we have recently reported on the Li insertion mechanism in view of long-range Coulombic interaction[12] and changes in electronic structure[15] by comparing the above two reactions.

To reveal the more detailed Li insertion mechanism, fundamental study on the crystal structure is needed. So far the crystal structure of thermally lithium inserted materials Li$_y$La$_{(1−y)/3}$NbO$_3$ has been investigated.[13,14,16,17] The crystal structure of pristine material, La$_{1/3}$NbO$_3$, was first described by Iymer and Smith.[16] As shown in Figure 1, La ions and vacancies at A-sites are ordered within alternate (001) planes doubling the *c* parameter of the cubic perovskite type cell and leading to a slightly distorted orthorhombic lattice with parameters $a \sim a_p$, $b \sim a_p$, and $c \sim 2a_p$ (subscript "p" refers to the cubic perovskite unit cell). According to Belous et al.,[13] the crystal symmetry changed from orthorhombic to tetragonal and then to cubic with increasing composition *y* in Li$_y$La$_{(1−y)/3}$NbO$_3$. In our previous study,[14] powder X-ray diffraction patterns of the samples $y \leq 0.05$ were indexed in an orthorhombic system. In the composition $y \geq 0.1$ the crystal structure changes to the tetragonal system, and then all the lattice parameters *a*, *b*, and *c* become equal at the composition $y = 0.25$. The peak intensity of superlattice (0 0 1/2)$_p$ due to cation and vacancy ordering of A-sites along the *c*-axis decreases with the composition *y*. Therefore, it was expected that ordering of A-site cations are destroyed and randomly distributed at the A-site by the reaction. Recently, through an electron diffraction study,[17] the decreasing of ordered arrangement of cations seems to be explained by

* Corresponding author. Telephone: + 81 3 5734 2145. Fax: +81 3 5734 2146. E-mail: mwakihar@o.cc.titech.ac.jp.
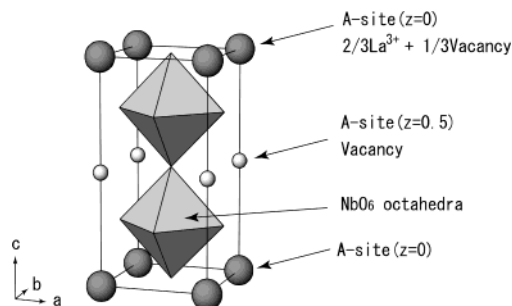
Figure 1. Crystal structure of $La_{1/3}NbO_3$.

Figure 2. Variation of potential with Li^+ insertion by quasi-equilibrium galvanostatic method for $Li_xLa_{1/3}NbO_3$.

the existence of a microdomain structure with three different orientations of the *c*-axis in the samples.

On the other hand, there is limited information on the crystal structure of electrochemically Li inserted material, $Li_xLa_{1/3}NbO_3$. Nadiri et al.[11] confirmed that the host structure of $La_{1/3}NbO_3$ is maintained during the insertion reaction, and reported lattice parameters with composition *x* using X-ray diffraction measurement. Dilanian et al.[18] investigated the crystal structure of chemically lithiated perovskite oxides, $Li_xLa_{1/3}NbO_3$, using neutron diffraction technique. Also, we have recently investigated the electrochemical behavior with Li insertion into the solid solution $Li_yLa_{(1-y)/3}NbO_3$ and concluded that the cell potential behavior with Li^+ insertion strongly depends on the arrangement of La^{3+} and Coulombic interaction.[12] These three reports[11,12,18] revealed that the inserted lithium ions reside at vacant A-sites. However, more detailed investigation of the crystal structure for the material with electrochemical lithium insertion is difficult due to experimental limitation, because the samples prepared by electrochemical reaction include another material, such as conductive additives and binder, in general. Therefore, the refinement of crystal structure, such as Rietveld refinement analysis using diffraction technique, cannot be applied to the material obtained by the electrochemical reaction. Despite such disadvantages, the extended X-ray absorption fine structure (EXAFS) technique is suited for studies on the crystal structure through electrochemical reaction since X-ray absorption only occurs at selected atoms. Some reports on the material with the electrochemical reaction using EXAFS measurement revealed the relevance for the structure analysis of such materials (for example, see refs 19−21). Furthermore, EXAFS technique provides short-range-order information around the target ions, or local lattice description, compared with a diffraction technique that offers only limited structural information on long-range order, or averaged lattice description.

In present study, we investigate the variation of interatomic distance with electrochemical Li insertion using EXAFS measurements to reveal the changes in local structure for $Li_xLa_{1/3}NbO_3$ as a function of the lithium content.

Experimental Section

$La_{1/3}NbO_3$ was prepared by a conventional solid-state reaction. As described in ref 14, the mixture of stoichiometric amounts of La_2O_3 (3 N), and Nb_2O_5 (3 N), (Soekawa Chemical Industries, Ltd.) was heated at 800 °C for 2 h and then at 1300 °C for 24 h in air with several intermittent grindings.

Electrochemical reaction of Li insertion was carried out using a three-electrode cell. Li foil (Aldrich) was used as the counter and reference electrodes, and 1 M solution of $LiClO_4$ in anhydrous ethylene carbonate (EC) and diethylene carbonate (DEC) was used as electrolyte (Tomiyama Pure Chemical Company, Ltd.). The working electrode was a mixture of 90 wt % perovskite powders, 7 wt % acetylene black as a current
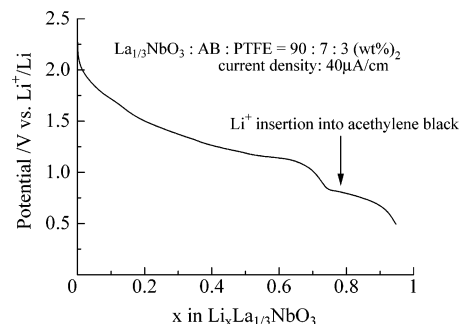
collector, and 3 wt % poly(tetrafluoroethylene) (PTFE) binder. Li foils and the mixture of the working electrode were pressed onto Ni mesh. The preparation of the samples with various compositions *x* was carried out by a galvanostatic method (current density 40 $\mu A/cm^2$) using a Hokuto HD-110mSM6 electrochemical interface. After the cell reaction, the electrode was washed in the solvent EC/DEC without electrolyte, and dried in a vacuum. The preparation of the cells and the electrochemical experiments were performed in an Ar-filled glovebox.

Crystalline phase identification for $Li_xLa_{1/3}NbO_3$ ($x = 0, 0.5, 0.7$) was carried out by powder X-ray diffraction (XRD) using a Rigaku RINT2500V diffractometer with Cu $K\beta$ radiation, and a curved graphite monochromator, and it was confirmed that the perovskite structure remains through the reaction. In this measurement, the sample was covered with polyethylene film in an Ar-filled glovebox to prevent reactions of the sample with moisture in the atomosphere.

Niobium K-edge X-ray absorption fine structure (XAFS) of samples, $Li_xLa_{1/3}NbO_3$, was measured by transmission mode using synchrotron radiation at BL-10B, Photon Factory, High Energy Accelerator Research Organization, Tsukuba, Japan, whereas lanthanum K-edge XAFS of the samples were measured at the BL-38B1 beam line, SPring-8, Japan Synchrotron Radiation Research Institute (JASRI), Hyogo, Japan. The samples after electrochemical treatment were pelletized with an appropriate amount of boron nitride binder and then sealed in a polyethylene bag to avoid exposure to air. The absorption of Cu K-edge was used for the calibration of the absolute energy scale. Energy selection was accomplished by using a monochromator with Si(311) crystals, and the X-ray intensity before and after sample was measured using ion chambers. The structural parameters were determined by curve-fitting procedures using REX2000 data analysis software.[22] Theoretical parameters of backscattering factors and phase shifts used in the curve-fitting analysis were calculated by FEFF7.[23]

Results

Figure 2 shows the cell potential under quite low galvanostatic current (40 $\mu A/cm^2$) through electrochemical lithium insertion. The detailed insertion site of lithium ion has already been reported in refs 12 and 18. The cell potential of the sample at the composition $x > 0.7$ is lower than 1.0 V, where lithium insertion into acetylene black would occur.[12] Therefore, the sample with $x > 0.7$ would correspond to being filled up with electrochemically inserted lithium ions at a vacant A-site.

Figure 3 shows the XRD diagrams for $Li_xLa_{1/3}NbO_3$ ($x = 0, 0.5, 0.7$). The peak features of the patterns were unchanged upon lithium insertion, indicating that the host structure of $La_{1/3}NbO_3$ keeps its framework as reported previously.[11] In detail, since
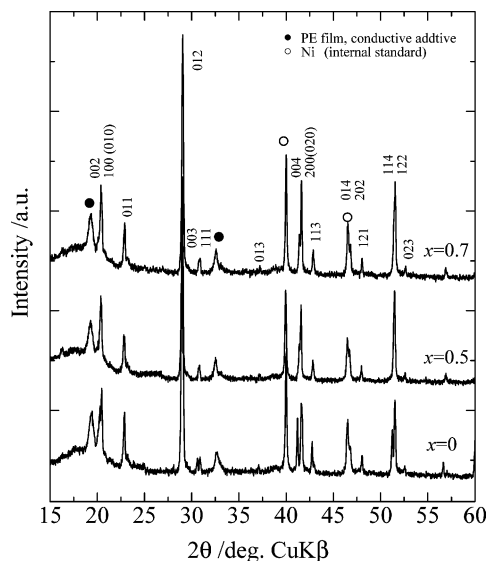
Figure 3. Variation of powder X-ray diffraction patterns of perovskite compounds Li$_x$La$_{1/3}$NbO$_3$ with electrochemical lithium insertion.

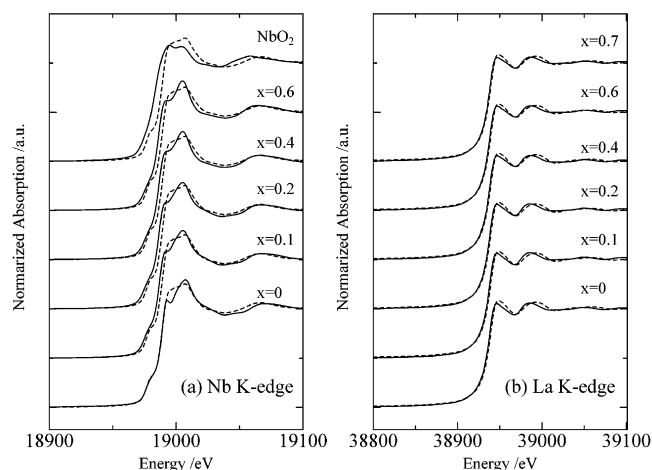**Figure 4.** (a) Nb K-edge XANES spectra for Li$_x$La$_{1/3}$NbO$_3$. Dashed line indicates XANES spectra of Nb$_2$O$_5$ as a reference material for Nb^{5+}. (b) La K-edge XANES spectra for Li$_x$La$_{1/3}$NbO$_3$. Dashed line indicates XANES spectra of La$_2$O$_3$ as a reference material for La^{3+}.

the peaks of (200) and (004) (or (114) and (122)) were incorporated with composition x, half the lattice parameter $c/2$ became closer to the lattice parameter a (Figure 1). According to the literature,[11] similar behavior has been already reported, and the ratio of lattice parameter $c/2a$ (indicating tetragonal deviation from cubic symmetry($c/2a = 1$)) varies a little from 1.022 ($x = 0$) to 1.008 ($x = 0.8$).

The Nb and La K XAFS spectra around the absorption edge, or X-ray absorption near edge structure (XANES), for the samples Li$_x$La$_{1/3}$NbO$_3$ are shown in Figure 4. The absorption energy of the parent material, La$_{1/3}$NbO$_3$ ($x = 0$), is consistent with that of Nb$_2$O$_5$, indicating that the oxidation state of Nb is +5. Then the Nb K-edge spectra shifted gradually to lower energy with composition x. Comparing with the XANES spectra of the reference samples, Nb$_2$O$_5$ (Nb^{5+}) and NbO$_2$ (Nb^{4+}), such behavior corresponds to the reduction of niobium ion from Nb^{5+} (parent sample, La$_{1/3}$NbO$_3$) to Nb$^{4.4+}$ (lithiated one with composition $x = 0.6$, Li$_{0.6}$La$_{1/3}$NbO$_3$). On the other hand, the absorption energies of La K-edge with various compositions x do not change and are identical to that of La$_2$O$_3$, indicating that the oxidation state of La remains +3 through the reaction. Hence, the electronic charge transference with lithium insertion

reaction mainly occurs not at the La ions, but at the Nb ions. This conclusion is consistent with our previous study using La L$_{III}$-edge, Nb L$_{III}$-edge, and O K-edge X-ray absorption spectra.[11]

The local structure of niobium and lanthanum ions in the perovskite Li$_x$La$_{1/3}$NbO$_3$ compounds has been quantitatively determined by using EXAFS spectroscopy. Fourier transforms (FTs) of the EXAFS oscillations yield a pseudoradial structure function (RSF) of the local atomic environment around the absorber atom. FTs of the k^3-weighted EXAFS oscillation for the samples were calculated in the range $k = 3.5-12$ (Nb K-edge) and $k = 3.5-13$ (La K-edge), respectively, since the EXAFS oscillation is clear enough to neglect the signal-to-noise error in this k range. The RSF of Nb K-edge EXAFS is presented in Figure 5a. The each peak of the RSF shown in Figure 5a is assigned by the theoretical calculation of RSF based on the structural parameters[16] using program code FEFF7.[23] The first peak at around 1.4 Å, the second one at around 3.2 Å, and the third one at around 3.4 Å correspond to the Nb−O, Nb−La, and Nb−Nb interactions, respectively. The Nb−Li interaction is negligible because of the low backscattering ability of the lithium. Note that the obtained interatomic distance in the figure showed much less than the expected one from the data of ionic radii,[24] because phase-shift corrections have not been applied to the RSF obtained by FT spectra presented. Like the case of Nb K-edge EXAFS, the RSFs of La K-edge EXAFS are shown in Figure 5b, and each peak is assigned by theoretical simulation. The first peak at around 2.1 Å, the second one at around 3.1 Å, and the third one at around 3.7 Å correspond to the La−O, La−Nb, and La−La interactions, respectively. Accurate structural information including the phase-shift corrections can be obtained by curve-fitting procedure concerning the simple single scattering of the photoelectron. The RSF data were inversely Fourier filtered (inverse-FT) over the first three peaks in the transformation (the ranges of inverse-FT are $0.58 \leq R \leq 4.14$ Å for Nb K-edge data and $1.57 \leq R \leq 4.08$ Å for La K-edge data). In the crystallographic view, each peak in the RSF (Figure 5) consists of several kinds of interaction having different interatomic distances. For example, the Nb−O pair includes one shorter Nb−O(1), four medium Nb−O(2), and one larger Nb−O(3) ion pairs from the data of XRD analysis.[16] In general, however, it is difficult to distinguish these bond lengths by EXAFS analysis because the k range for curve-fitted $\chi(k)$ spectra was limited ($3.5 \leq k \leq 12$ for Nb K-edge, or $3.5 \leq k \leq 13$ for La K-edge), and it would result in decrease of mathematical reliability in the curve-fitting procedure. Therefore, each peak observed in the RSF was regarded as one-shell, and we tried to perform the three-shell fitting: Nb−O, Nb−La, and Nb−Nb shells for Nb K-edge spectra; La−O, La−Nb, and La−La shells for La K-edge spectra.

The best fitting results are compared to the experimental spectra in Figure 6, and the fitted structural parameters are summarized in Tables 1 and 2. In the case of Nb K-edge spectra, the fitting results (Figure 6a) show a little deviation from the observed inverse-FT spectra. Such a deviation might be due to the ignorance of high order cumulant representing the anharmonic effect in the interatomic potential, or due to that of multiple scattering (MS) effects, such as Nb−O−O and Nb−O−Nb three-body signals. The curve fittings taking into account the third and forth cumulant parameters were also performed. The refined parameters of interatomic distances and Debye−Waller factors are almost the same as those refined values without cumulant parameters, and these refined cumulant parameters are quite small. Therefore, the high order cumulant effects[24] can be neglected in this study. MS effects were
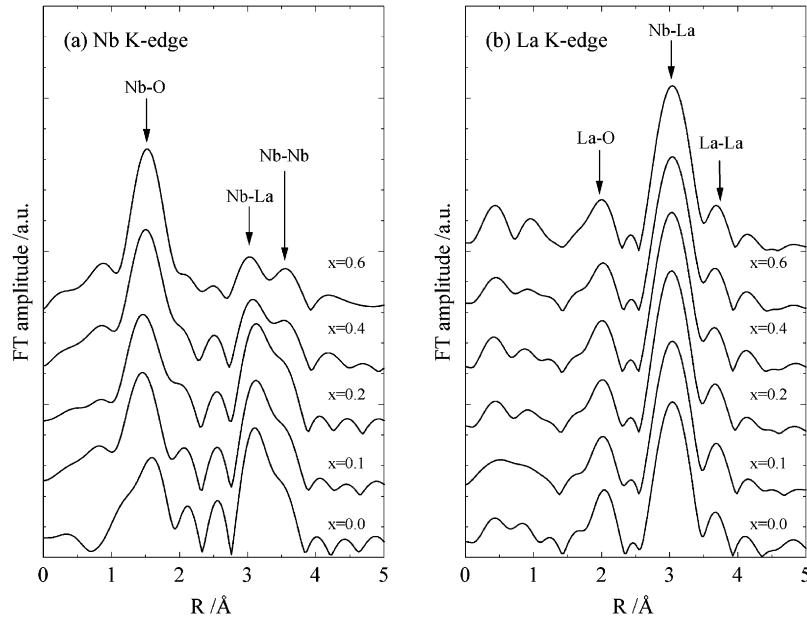
Figure 5. Radial structure functions (RSF) for perovskite samples around (a) Nb and (b) La atom resulting from Fourier transform (FT) EXAFS oscillation.
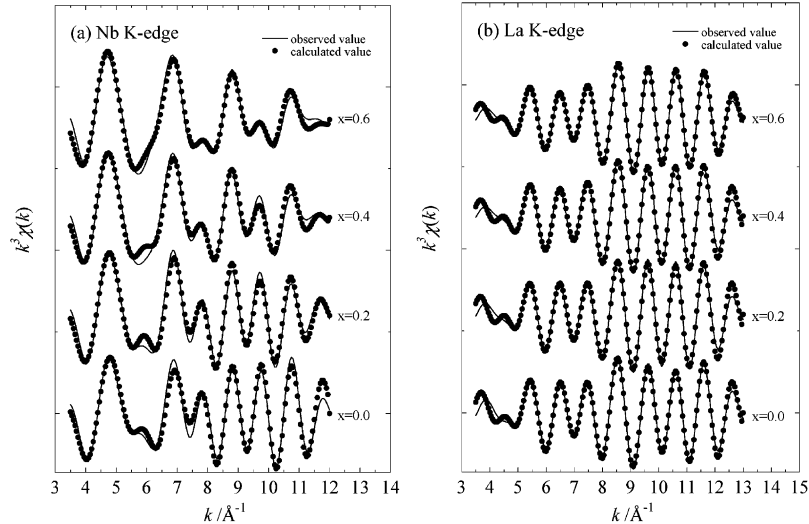

Figure 6. Typical results of curve-fitting procedure for inverse FT spectra. (a) Inverse FT of RSF for Nb K-edge; (b) that for La K-edge.

TABLE 1: Obtained Structural Parameters, Coordination Number (CN), Interatomic Distance (R), and Debye−Waller Factors (σ), by Nb K-edge EXAFS for Perovskite Oxides, $Li_xLa_{1/3}NbO_3$

	Nb−O			Nb−La			Nb−Nb			
x	CN	R/Å	σ/Å	CN	R/Å	σ/Å	CN	R/Å	σ/Å	residue[a]/%
0	6[b]	1.953	0.108	2.67[b]	3.481	0.061	6[b]	3.931	0.131	5.97
0.1	6[b]	1.962	0.094	2.67[b]	3.489	0.077	6[b]	3.950	0.121	2.97
0.2	6[b]	1.975	0.095	2.67[b]	3.488	0.080	6[b]	3.965	0.117	4.32
0.4	6[b]	1.992	0.083	2.67[b]	3.495	0.093	6[b]	3.962	0.125	4.37
0.6	6[b]	2.005	0.081	2.67[b]	3.496	0.106	6[b]	3.951	0.127	3.56

[a] Residue = $100\sum\{k^n\chi_{obs}(k) - k^n\chi_{cal}(k)\}^2/\sum\{k^n\chi_{obs}(k)\}^2$. [b] Fixed parameter for the curve-fitting procedure.

estimated by the simulation using FEFF7 code.[23] In the case of La K-edge spectra, there is no MS effect in the range of the nearest three peaks in the RSF signal. On the other hand, in the case of Nb K-edge spectra, three-body scattering of 180° Nb−Nb−O about 4 Å (which is consistent with third shell of Nb−Nb interaction) might contribute to the spectra to some extent. However, since the simulation results neglected Debye−Waller factors and local distortion of ion arrangement which decrease the EXAFS oscillation of multiple scattering drastically, the dominant contributions to the total EXAFS oscillation are made

by the two-body single scattering signals (at least with regard to the first two shell, Nb−O and Nb−La). Furthermore, the residue of fitting results is less than 6%, and the Nb−La interatomic distance obtained by both of Nb K-edge and La K-edge EXAFS spectra is consistent within experimental error. Hence we judged that reliable values, especially of the interatomic distance, were obtained in this fitting procedure.

Compositional dependence of interatomic distances is presented in Figure 7. The interatomic distance of the first shell Nb−O (Figure 7a) monotonically increased with composition

TABLE 2: Obtained Structural Parameters, Coordination Number (CN), Interatomic Distance (R), and Debye−Waller Factors (σ), Using La K-edge EXAFS for Perovskite Oxides, Li$_x$La$_{1/3}$NbO$_3$

	La−O			La−Nb			La−La			
x	CN	R/Å	σ/Å	CN	R/Å	σ/Å	CN	R/Å	σ/Å	residue[a]/%
0	12[b]	2.553	0.092	8[b]	3.497	0.065	2.67[b]	3.869	0.054	2.29
0.1	12[b]	2.548	0.115	8[b]	3.497	0.065	2.67[b]	3.890	0.078	3.06
0.2	12[b]	2.550	0.104	8[b]	3.496	0.063	2.67[b]	3.893	0.077	3.09
0.4	12[b]	2.535	0.099	8[b]	3.495	0.063	2.67[b]	3.907	0.089	2.49
0.6	12[b]	2.527	0.091	8[b]	3.504	0.065	2.67[b]	3.934	0.069	1.21
0.7	12[b]	2.515	0.101	8[b]	3.482	0.065	2.67[b]	3.910	0.065	2.00

[a] Residue = $100\sum\{k^n\chi_{obs}(k) - k^n\chi_{cal}(k)\}^2/\sum\{k^n\chi_{obs}(k)\}^2$. [b] Fixed parameter for the curve-fitting procedure.
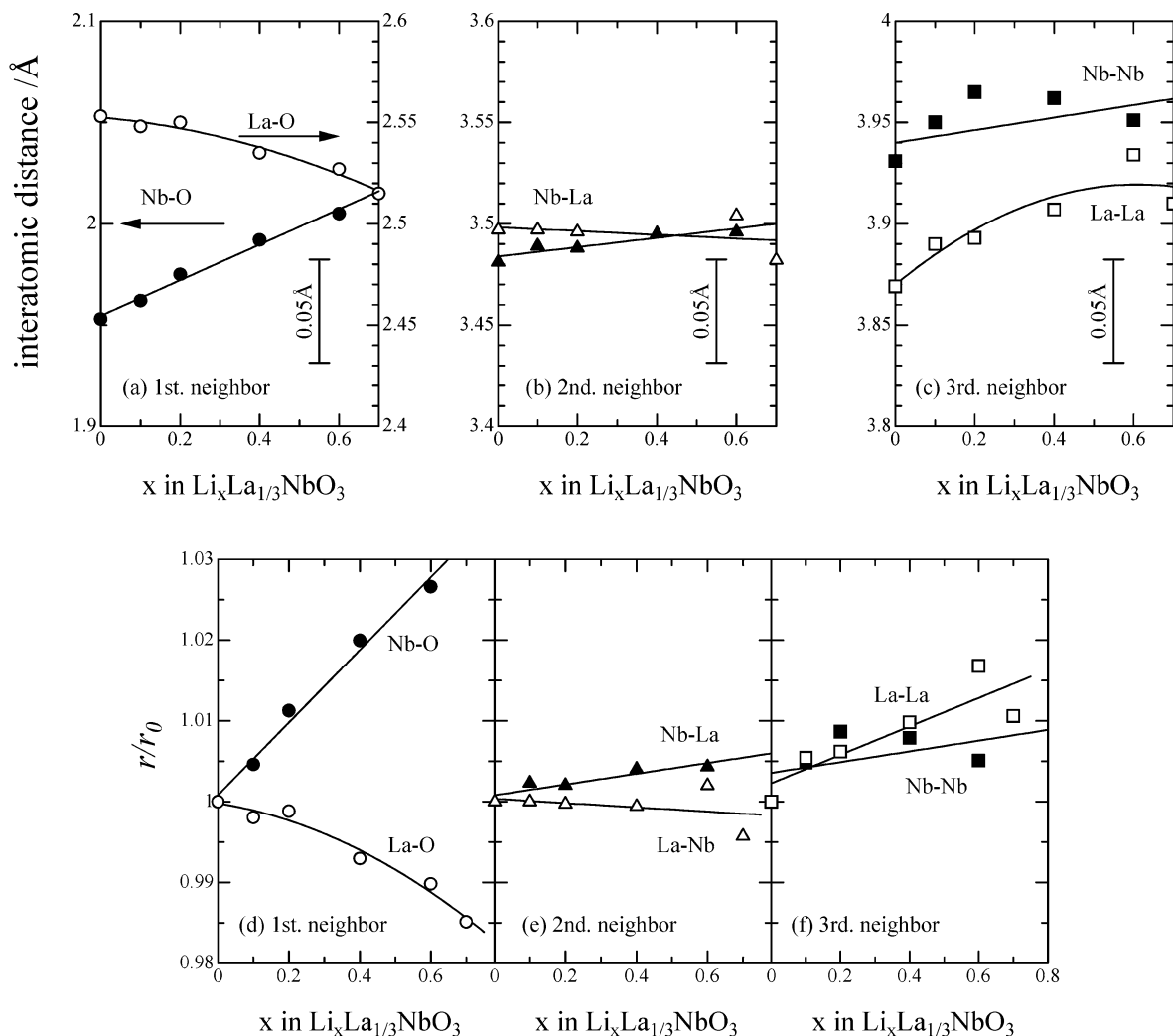

Figure 7. Compositional dependence of interatomic distance changes: (a) first neighbor interaction, Nb−O and La−O; (b) second neighbor interaction, La−Nb; and (c) third neighbor interaction, La−La and Nb−Nb. Open and solid symbols show the obtained data from Nb K-edge and La K-edge EXAFS spectra, respectively. For comparison, the interatomic distances were replotted in (d)−(f) with respect to the r/r_0 value, where r and r_0 indicate the interatomic distance of each bond and that of the parent material, La$_{1/3}$NbO$_3$, respectively.

x, resulting from the reduction of niobium ion as mentioned in Figure 4a and which originates from the expansion of ionic radii.[25] On the other hand, that of the first shell La−O tends to decrease with composition x as shown in Figure 7a. Figure 7b shows that the interatomic distance of second shell interaction, Nb−La (or La−Nb), tends to be unchanged through the Li insertion reaction. In the case of third shell interaction, Nb−Nb and La−La (Figure 7c), which directly associated with the cell dimension, shows a small amount of increase with the reaction. This would reflect the fact that the cell volume reported by Nadiri et al.[11] expands slightly during the insertion reaction (only shows a little expansion, ∼0.3%, from $x = 0$ to 0.8 in Li$_x$La$_{1/3}$NbO$_3$).

For the comparison of a certain interatomic distance with another shell's one, the relative bond length r/r_0 is calculated, where r indicates the interatomic distance listed in Tables 1 and 2, and r_0 is that of the parent material, La$_{1/3}$NbO$_3$, since it is not adequate to compare those obtained data itself (for example, assuming the isotropic expansion, the variation of Nb−Nb interaction is twice as large as that of Nb−O interaction). The results are plotted in Figure 7d−f. From this figure, it is concluded that the interatomic distances of first coordination shells changed more drastically than second and third ones with lithiation (increase in Nb−O pair and decrease in La−O pair).
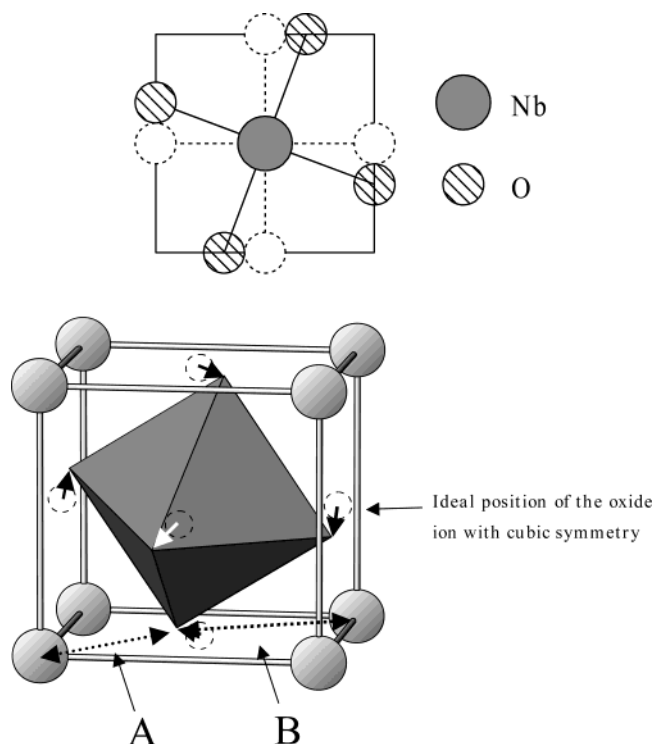
10720 *J. Phys. Chem. B, Vol. 107, No. 39, 2003*

Nakayama et al.

Figure 8. Schematic image of one of the possible arrangements of ions with NbO$_6$ octahedral tilting. (a) (200) projection of perovskite structure; solid line indicates the tilting structure and dashed one is the atomic arrangement with cubic symmetry. (b) Three-dimensional description. The picture only reflects the local structure around Nb ions without consideration of the periodicity for crystal symmetry. The solid arrows indicate the shift of oxide ion from ideal position with cubic symmetry. The dashed arrows show the examples of La–O interatomic distance after lithiation.

Discussion

In this section, we discuss the changes of local structure in Li$_x$La$_{1/3}$NbO$_3$ in view of the variation of the interatomic distance. Although there are no marked structural changes, or rearrangement of host lattice framework (Figure 2 and ref 11), the experimental results summarized in Figure 7 and Tables 1 and 2 were quite complicated, because each interatomic distance shows different behavior with the depth of lithiation: increase of Nb–O, decrease of La–O, identical to Nb–La, slight increase of Nb–Nb and La–La pairs, respectively. In these ion pairs, Nb–O pair shows the most appreciable increase. It can be understood through the following explanation. Through the lithiation, the niobium ions reduce their oxidation state from +5 to +4 (Figure 4) and expand their ion sizes due to the weakening of the shielding effect (Nb^{5+}, 0.64 Å; Nb^{4+}, 0.68 Å).[25] Therefore, the increasing Nb–O interatomic distance (Figure 4) can be understood in view of the reduction of Nb ion. However, the unit cell size is almost the same before and after the reaction despite the expansion of Nb–O bond (Figure 7f and ref 11).

To explain such behavior, we proposed the model based on the tilting of NbO$_6$ octahedra in the reaction. Figure 8 shows a simple schematic image of the NbO$_6$ octahedral tilting model. The figure briefly shows the octahedral tilting model in the case of the perovskite with cubic symmetry ($Pm\bar{3}m$). Note that the more accurate symmetrical and/or crystallographic description of tilting including the long-range periodicity cannot be evaluated by the EXAFS measurement because this method only provides one-dimensional radial structural information. However, the possible arrangement of such perovskites with

octahedral tilting is limited due to the constraint of translational symmetry operation. The detailed classification of tilted octahedral with crystal symmetry in perovskites were already reported by Glazer.[26] In this model, since the oxide ion gradually shifts its position upon reduction of niobium (accompanying lithium insertion), the interatomic distance of Nb–O increases (see Figure 8). On the other hand, the arrangement of both cations at the A-site and B-site is unchanged before and after lithiation, indicating that interatomic distances of Nb–La, Nb–Nb, and La–La show constant values. Therefore, the model accounts for the observed structural changes of the following interatomic distances (Figure 7): (i) increase of Nb–O interaction and (ii) unchanged or slight increase of Nb–La, Nb–Nb, and La–La interaction, respectively. Especially, the latter interactions of Nb–Nb and La–La correspond to the lattice parameter of the perovskite structure (see Figures 1 and 8), and the slight increases of these interactions observed in the EXAFS analysis are consistent with the small expansion of lattice parameters measured by X-ray diffraction technique.[11] Finally, we discuss the changes of La–O interatomic distance. As shown in Figure 8b, the La–O interatomic distance changes in a different manner, and depends on the tilting directions. Some of the bond would decrease, while the others increase (for example, see the dashed arrows A and B in Figure 8b). One explanation for the decreases of La–O interatomic distance may be given as follows. The NbO$_6$ octahedra would tilt toward the lanthanum ion selectively due to the short-range attractive interaction between lanthanum and oxygen, such as Coulombic attraction. However, the evidence for such attractive interaction is still insufficient.

From a different standpoint, the explanation for the changes of each interatomic distance associated with octahedral tilting would be also supported by the relationship of cation sizes in the perovskite structure. There are a large number of reports to describe the octahedral tilting mechanism in perovskite structures using the phenomenological or semiempirical models.[26–29] For example, the octahedral tilting was classified by the ionic radii (r(A) and r(B)) or polyhedral volume (V(AX$_{12}$) and V(BX$_6$)) for the perovskite ABX$_3$. The tolerance factor t[30] is a useful index for the geometric relationship of atomic positions in the perovskite structure. The tolerance factor t is defined by

$$t = \frac{r(A) + r(X)}{\sqrt{2}\{r(B) + r(X)\}} \tag{3}$$

where r(A), r(B), and r(X) indicate the ionic radii of the perovskite A-site, B-site, and anion, respectively. In $t = 1$, which is a geometric condition for a closed packing system, it is known that the arrangement of ions in the perovskite structure tends to be an ideal one with cubic symmetry ($Pm\bar{3}m$), and the structure distorts with decreasing t. In the case of pristine material, La$_{1/3}$NbO$_3$, the estimated tolerance factor t is 0.957 from the data of Shanon's ionic radii[24] (r(A=La^{3+}) = 1.36 Å, r(B=Nb^{5+}) = 0.64 Å, r(X=O^{2-}) = 1.40 Å), and decreases with lithium insertion because of increasing ionic radii (r(B=Nb^{4+}) = 0.68 Å). Therefore, the structure deviates from the closed packing. However, since the perovskite oxides tend to keep the dense structure, the perovskites do not expand isotropically, but NbO$_6$ octahedra may tilt as shown in Figure 8.

To our knowledge, this is the first indication that the tilting of octahedra in perovskite could be controlled by electrochemical reaction. Such a tilting control causes the symmetrical change of crystal structure. It is well-known that various physical properties (such as electrical property, optical property, and so

forth) depend on the crystal symmetry. Therefore, our proposed model may provide a new method to control the physical and/or chemical properties of perovskite type materials in the future.

Conclusion

The changes of oxidation states of cations and local structure of Li$_x$La$_{1/3}$NbO$_3$ with electrochemical lithium insertion have been investigated using XAFS measurements. From the Nb and La K-edge XANES spectra, the Nb cations reduce their oxidation state from +5 to +4, and the oxidation state of La cations remains unchanged with composition x. Accompanying the reduction of niobium ion, the interatomic distances of Nb−O, La−O, and higher shell contribution (Nb−La, Nb−Nb, and La−La) are increasing, decreasing, and unchanged, respectively. Such a complicated behavior could be attributed to the tilting of the NbO$_6$ octahedra with reaction.

References and Notes

(1) Scrosati, B. *Nature* **1995**, *573*, 557.

(2) Wakihara, M.; Guohua, L.; Ikuta, H. *Lithium Ion Batteries*; Kodansha: Tokyo, 1998; Chapter 2.

(3) Zheng, T.; Dahn, J. R. *Phys. Rev. B* **1997**, *56*, 3800.

(4) Aydinol, M. K.; Kohan, A. F.; Ceder, G.; Cho, K.; Joannopoulos, J. *Phys. Rev. B* **1997**, *56*, 1354.

(5) Koyama, Y.; Kim, Y.-S.; Tanaka, I.; Adachi, H. *Jpn. J. Appl. Phys.* **1999**, *38*, 2024.

(6) Hibino, M.; Han, W.; Kubo, T. *Solid State Ionics* **2000**, *135*, 61.

(7) Liu, Y.; Fujiwara, T.; Yukawa, H.; Morinaga, M. *Electrochim. Acta* **2001**, *46*, 1151.

(8) Gao, Y.; Reimers, J. N.; Dahn, J. R. *Phys. Rev. B* **1996**, *54*, 3878.

(9) Goodenough, J. B.; Manthiram, A.; Wnetrzewski, B. *J. Power Sources* **1993**, *43−44*, 269.

(10) Yamaki, J.; Egashira, M.; Okada, S. *J. Power Sources* **2001**, *97−98*, 349.

(11) Nadiri, A.; Le Flem, G.; Delmas, C. *J. Solid State Chem.* **1988**, *73*, 338.

(12) Nakayama, M.; Imaki, K.; Ikuta, H.; Uchimoto, Y.; Wakihara, M. *J. Phys. Chem. B* **2002**, *106* (25), 6437.

(13) Belous, A. G.; Novitskaya, G. N.; Polyanetskaya, S. V.; Gornikov, Yu, I. *Izv. Akad. Nauk SSSR, Neorg. Mater.* **1987**, 470.

(14) Kawakami, Y.; Ikuta, H.; Wakihara, M. *J. Solid State Electrochem.* **1998**, *2*, 206.

(15) Nakayama, M.; Imaki, K.; Ra, W.-K.; Ikuta, H.; Uchimoto, Y.; Wakihara, M. *Chem. Mater.* **2003**, *15*, 1728.

(16) Iyer, P. N.; Smith, A. J. *Acta Crystallogr.* **1967**, *23*, 740.

(17) Garcia-Martin, S.; Alario-Franco, M. A. *J. Solid State Chem.* **1999**, *148*, 93.

(18) Dilanian, R. A.; Yamamoto, A.; Izumi, F.; Kamiyama, T. *Mol. Cryst. Liq. Cryst.* **2000**, *341*, 225.

(19) Nakai, I.; Yasaka, K.; Sasaki, H.; Terada, Y.; Ikuta, H.; Wakihara, M. *J. Power Sources* **2001**, *97−98*, 412.

(20) Shiraishi, Y.; Nakai, I.; Tsubata, T.; Himeda, T.; Nishikawa, F. *J. Solid State Chem.* **1997**, *133*, 587.

(21) Hara, D.; Shirakawa, J.; Ikuta, H.; Uchimoto, Y.; Wakihara, M.; Miyanaga, T.; Watanabe, I. *J. Mater. Chem.* **2002**, *12*, 3717. Hara, D.; Shirakawa, J.; Ikuta, H.; Uchimoto, Y.; Wakihara, M.; Miyanaga, T.; Watanabe, I. *J. Mater. Chem.* **2003**, *13,* 897.

(22) Rigaku EXAFS Analysis Software, REX2000; Catalogue No. 2612S311/312/321/322, Rigaku Co., 2000.

(23) Multiple-scattering XAS simulation code: Ankudinov, A. L.; Ravel, B.; Rehr, J. J.; Conradson, S. D. *Phys. Rev. B* **1998**, *58*, 7565. Ankudinov A. L.; Rehr, J. J. *Phys. Rev. B* **1997**, *56*, R1712. Zabinsky, S. I.; Rehr, J. J.; Ankudinov, A.; Albers, R. C.; Eller, M. J. *Phys. Rev. B* **1995**, *52*, 2995. For further details see, for example, the documentation at the URL: http://leonardo.phys.washington.edu/feff/

(24) Ishii, T. *J. Phys.: Condens. Matter* **1992**, *4*, 8029.

(25) Shannon, R. D. *Acta Crystallogr., Sect. A* **1976**, *A32*, 751.

(26) Glazer, A. M. *Acta Crystallogr., Sect. B* **1972**, *B28*, 3384.

(27) Woodward, P. M. *Acta Crystallogr., Sect. B* **1997**, *B53*, 44.

(28) Magyari-Köpe, B.; Vitos, L.; Johansson, B.; Kollár, J. *Phys. Rev. B* **2002**, *66*, 092103.

(29) Howard, C. J.; Stokes, H. T. *Acta Crystallogr., Sect. B* **1998**, *B54*, 782.

(30) Golschmidt, V. M. *Soil Sci.* **1945**, *60*, 1.